Sains Malaysiana 51(2)(2022): 405-419
http://doi.org/10.17576/jsm-2022-5102-07

New Empirical Approach for the Estimation of Soil Cohesion and Friction Angle in 2D Form for Site Investigations

(Pendekatan Empirik Baru terhadap Anggaran Persepaduan Tanah dan Sudut Geseran dalam Bentuk 2D untuk Kajian Lapangan)

BALA BALARABE, ANDY ANDERSON BERY*, TEOH YING JIA & AMIN ESMAIL KHALIL

ABSTRACT

This paper presents the multiple linear regression (MLR) models developed from electrical resistivity and seismic refraction surveys for quick prediction of subsurface soil's shear strength parameters. A total of four parameters have been considered with electrical resistivity and seismic refraction velocity as the independent variables: and soil cohesion and internal friction angle as the dependent variables. In order to mitigate the effects of nonlinearity of resistivity and velocity, both datasets were initially log-transformed to conform with the fundamental assumptions of regression analysis. Two models were therefore built based on the strong multiple linear relationships between explanatory and response variables, with coefficient of determination (R^2), 0.777, p-values, < 0.050, Durbin-Watson value, 1.787 and multicollinearity, 1.185. The obtained models' coefficients were transferred and used for the estimation of 2D models soil cohesion and internal angle of friction for validation. Thereafter, the developed models demonstrated good performance, having subjected to accuracy assessment with results at < 5%, and < 10% for the root mean square error (RMSE) and weighted mean absolute percentage error (MAPE) respectively. Therefore, the new developed soil's shear strength MLR models have provided continual description of soil properties in two-dimensional form, enhancing the subsurface information for site investigations as compared, to one-dimensional information from the invasive method.

Keywords: Land uses; refraction; regression; resistivity; shear strength

ABSTRAK

Kajian ini membentangkan model regresi linear berganda (MLR) yang dibangunkan daripada tinjauan kerintangan elektrik dan pembiasan seismik untuk meramalkan parameter kekuatan ricih bagi permukaan bawah tanah. Sebanyak empat parameter telah dipertimbangkan dengan halaju kerintangan elektrik dan biasan seismik sebagai pemboleh ubah tidak bersandar: dan persepaduan tanah dan sudut geseran dalaman sebagai pemboleh ubah bersandar. Untuk mengurangkan kesan tidak kelinearan kerintangan dan halaju, kedua-dua set data pada mulanya diubah log untuk mematuhi andaian asas analisis regresi. Oleh itu, kedua-dua model dibina berdasarkan hubungan linear berganda yang kuat antara pemboleh ubah penjelasan dan tindak balas, dengan pekali penentuan (R^2), 0.777, nilai-p, < 0.050, nilai Durbin-Watson, 1.787 dan multikolineariti, 1.185. Pekali model yang diperoleh telah dipindahkan dan digunakan untuk menganggarkan persepaduan tanah model 2D dan sudut geseran dalaman untuk pengesahan. Kemudian, model yang dibangunkan menunjukkan prestasi yang baik, setelah tertakluk kepada penilaian ketepatan dengan keputusan pada < 5 dan < 10% masing-masing untuk ralat purata kuasa dua akar (RMSE) dan ralat peratusan mutlak purata berpemberat (MAPE). Oleh itu, model MLR kekuatan ricih tanah yang baru dibangunkan telah memberikan penerangan berterusan tentang sifat tanah dalam bentuk dua dimensi, maklumat bawah permukaan tanah untuk kajian tapak berbanding dengan maklumat satu dimensi daripada kaedah invasif.

Kata kunci: Biasan; kegunaan tanah; kekuatan ricih; kerintangan; regresi

INTRODUCTION

Subsurface geological instabilities and failures are often attributable to a continuous degradation of strength properties of soils which may lead to damages of design and engineering structures. Many soil collapses/failures encompass a shear-type failure because of the nature of soil. The incidence of soil degradation is commonly linked to the weakening of core soil interconnecting particles, thus, the shear strength parameters are basic criteria showing the capability of soils to withstand shear destruction (Guo &

Zhao 2013). A soil is comprised of separate soil particles which slip adjacently whenever soil carries a load. Soil's shear strength is needed in various kinds of engineering analysis, for instance, the bearing capacities of both near and deep foundations, slope stability analysis, designs, and construction of retaining walls (Shahangian 2011). Strength of soil is a vital non-unique parameter and could vary periodically based on the present of stress (Mitchell & Soga 2005). Estimating and monitoring strength of soil/soil variability in a quick and comprehensive manner that could lead to collapse and damages of structures is essential, especially when erecting high rising buildings. Invasive and bon-invasive techniques are applied in the calculation/estimation of the geotechnical subsurface data of soil strength parameters. Invasive techniques for instance probe drillings for excavation projects and boring (e.g. percussion drillings and power auguring) from ground-surface depend on the collected *in-situ* geotechnical data. The techniques could offer data with high accuracy due to direct contact to raw soil and rock units/samples, however, are costly, limited data coverage and labor-intensive. Conversely, the non-invasive techniques have better data coverage, minimal damage level, great speed and less expensive, however, have limited access to the rock units, thus the precision is usually lesser compared to that of invasive techniques. To obtain correct and reliable soil's shear strength estimation models, the initial stage was to deploy non-destructive techniques on marked profile lines and then followed by collection of few soil samples for geotechnical laboratory analysis using invasive techniques. The approach seeks to improve the accuracy of the sampled points/exploration positions (Alimoradi et al. 2008), with less cost and minimal environmental damages (Owusu-nimo & Boadu 2020).

The electrical resistivity imaging is a non-invasive technique method normally employed to determine properties of geological materials (soil/rocks) with varied subsurface conditions, in a wide range of applications such as groundwater investigation (Yeh et al. 2015), geological body imaging (Nguyen et al. 2005), and geotechnical assessments (Caterina et al. 2013; Ismail et al. 2019). So many parameters for instance soil/rock-types, saturations, porosities, and fluid-conductivity are influenced by electrical resistivity, given the method vast applicability. The electrical resistivity surveys save time, less cost with computerized multichannel and switching systems (Van Hoorde et al. 2017). Utilizing the technique in correlation with laboratory results offers significant subsurface information for several geologic bodies and soil/rock units.

Seismic refraction tomography is one the geophysical methods capable of elucidating the geologic settings in regions whereby direct techniques such as drillings are impracticable due to challenges like limitation and economic constraint (Martínez & Mendoza 2011). The method is used to determine important compressional velocity (p-wave) information for a great subsurface volume in 2- dimension. Refraction velocity influences some geotechnical parameters like porosities, Poisson-ratio, shear, and elastic moduli. The understanding of the elastic parameters of the geomaterials based on the study of seismic-wave propagation has increased importance in the engineering fields of geology and geotechnics (Junior et al. 2012). The shallow refraction tomographic method is a dynamic geophysical technique with several field applications as it allows the search for an investigation of the course of boundaries, thereby aiding to address issues related to geological, environmental, geotechnical, engineering (Brixova et al. 2018; Mcclymont et al. 2016; Shtivelman 2003); hydrogeological investigations (Gabr et al. 2012); and archaeological studies (Shahrukh et al. 2012); landslides monitoring and ground stability assessments (Whiteley et al. 2020; Wu et al. 2018). The method is very effective for subsurface site characterizations, especially in the evaluation of geotechnical parameters of reclaimed areas (Adewoyin et al. 2021). It is in simple operation with great-speed data measurement system and better precision in detection of geologic structure.

The values of parameters (resistivity and velocity) embraced in both electrical resistivity and seismic refraction imaging techniques are susceptible to various kinds of soil/rock properties and inhomogeneities that prevail beneath the investigated area (subsurface), for example, the resistivity method is susceptible to clay-content and pore-fluid, while the refraction seismic is susceptible to moisture content in soils/pore fluid in saturated rocks, lithological and physical properties of materials.

The present work attempts to integrate electrical resistivity and seismic refraction velocity models, using multiple linear regression (MLR) approach, to develop and assess empirical models for rapid 2D computation of soil cohesion and internal friction angle. This approach can provide 2D description of soils' strength properties at subsurface with minimal environmental influence compared to the conventional geotechnical methods. Beside recognizing the dynamism and problems-solving capability of regression procedure, the study takes its novelty in its effort to be the first in developing simple regression empirical 2D models for the estimation of

subsurface soil cohesion and internal friction angle from integration of electrical resistivity and seismic refraction velocity datasets. The approach can serve as a proxy platform through which fast 2D estimation of soil cohesion and internal friction angle can be achieved without opting to sophisticated constrained/ joint inversion schemes and destructive traditional geotechnical methods.

GEOLOGICAL SETTINGS

The study was carried out in Penang Island located at North West of Peninsular Malaysia. Penang Island being among the most rapidly developed regions of Malaysia, is characterized by normal temperature variation between 29 and 35 °C annually with upward rise in April and June. Pradhan and Lee (2010) reported that the Island experienced mean relative humidity of 65 to 95% and monthly rainfall of 240 to 58.6 mm. However, June and September of every year tend to record very low mean relative humidity. The major rock type in the area is granite and was categorized due to the degree of alkali type of feldspars to overall feldspars present in the area (Ahmad et al. 2006). In the northern segment, the dominant feldspars comprise of alkali feldspars with orthoclase to median microcline, not displaying well-defined *cross*hatch twinning pattern while in the

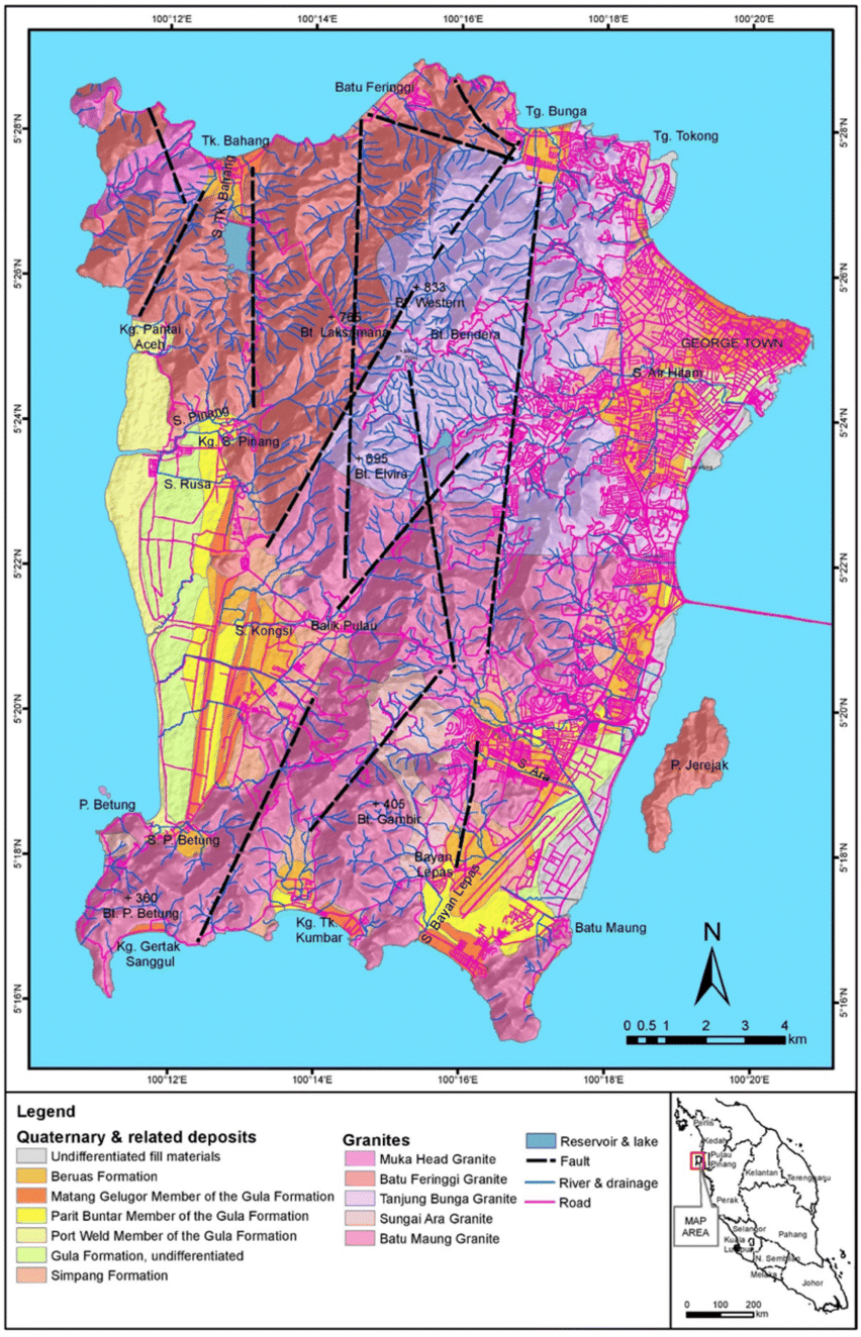

FIGURE 1. Geological map of Penang Island, Malaysia (Abdul Hamid et al. 2019)

southern segment, clear-cut crosshatch twining patterns of microcline are conspicuous (Ong 1993). Figure 1 displays simple geological map of the Island indicating the study segment.

Materials and Methods

2-D resistivity and seismic refraction methods

The approach offered in this study utilizes multiple linear regression technique as a proxy tool for joining of individualistically gotten tomographic models of electrical resistivity and seismic refraction velocity, with an effort to generate 2D pseudo sections of the soil cohesion and internal friction angle. The parameters of soil strength, cohesion and internal friction angle have been used in civil engineering projects and environmental studies, to estimate the degree of variations in shear strength of soils. Especially, the variability of hydrological situations which is not unusually the basic feature in changing the attractive forces in particles, hence impacting on shear strength values (Horn 2003; Wei et al. 2019). The datasets used for the regression modelling were acquired by both electrical resistivity and seismic refraction surveys (Figure 2). For 2D resistivity, ABEM SAS4000 equipment was used, and

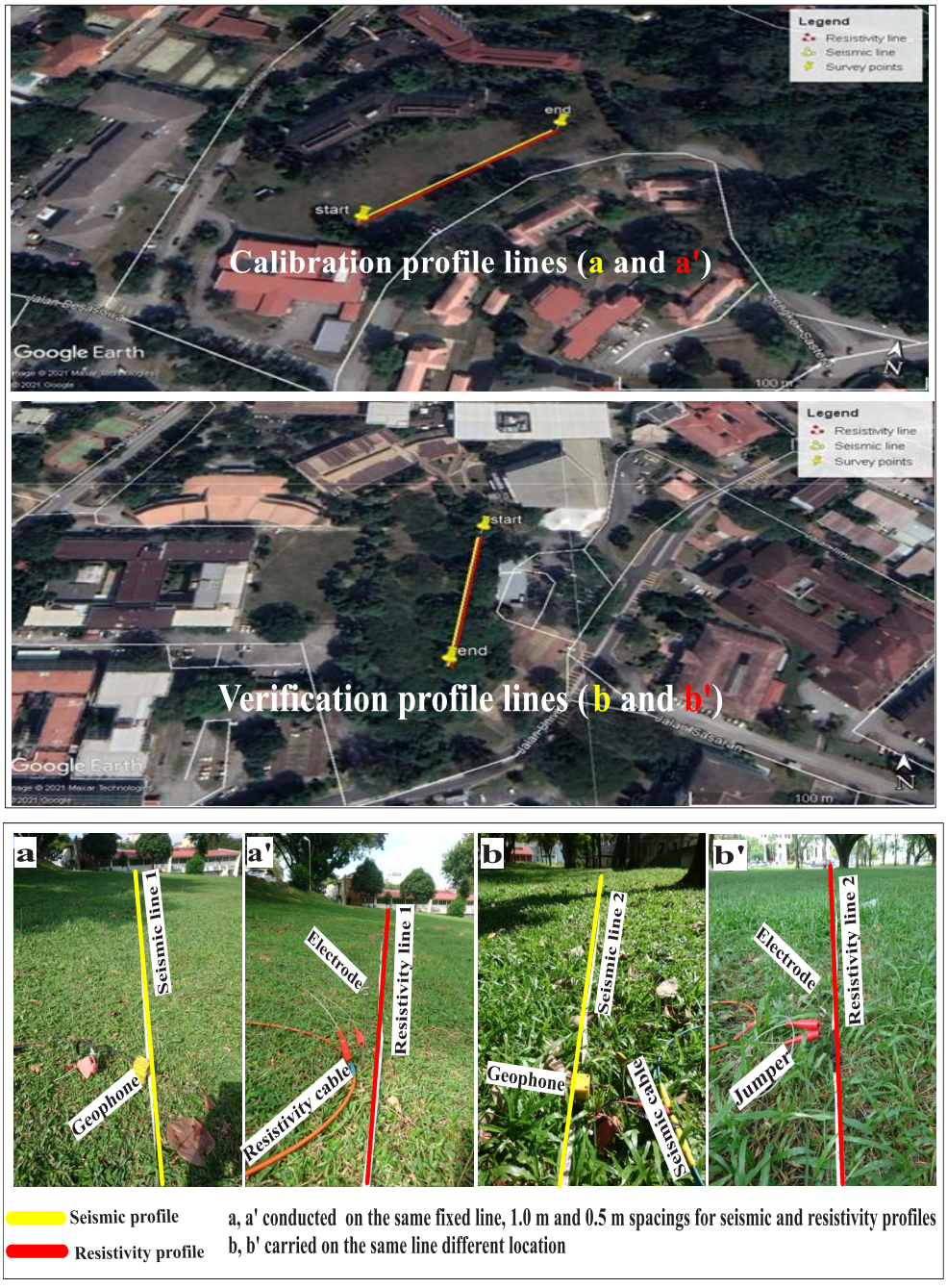

FIGURE 2. Google earth and field photos of seismic and resistivity profile survey lines (a, a') and (b, b') profiles used for both model calibration and verification at Minden and Batu Uban areas, respectively

two profile lines established. Among all the different resistivity array types, Wenner-Schlumberger array was employed due to its potential in resolving vertical and horizontal subsurface resistivity changes. Of the two profiles, each profile contained 41 planted electrodes at spacing of 0.5 m, fastened to two survey cables, take-outs, and jumpers for measurements. As reported by Okpoli (2013), that good horizontal resistivity resolution is highly possible by small electrode spacings than larger spacings. A Terrameter coupled with the equipment measures voltage automatically for every four planted electrodes and computes the apparent electrical resistivity based on a set current of 100 mA and 2 stacking.

The calculated apparent electrical resistivity data points are organized in a systematic manner that every given point is described with its coordinate values. These data values are converted into RES2DINV software format in preparation for filtering and inversion processes. The data values are therefore checked and filtered to avoid bad data values that might cause misinterpretations. Thereafter, all the data values are inverted by standard constraint least-squares (SCLS) inversion scheme existing in RES2DINV scheme. The software computes the apparent resistivity data values and makes comparison with the measured data values, repeatedly by adjustment until, the computed apparent resistivity model matches up the measured apparent resistivity model (Loke & Barker 1996). The repetition process is then halted when the percentage change between root mean squares (RMS) errors falls to acceptable range. Finally, the true subsurface resistivity models are produced and contoured accordingly.

Seismic refraction is one of the geophysical methods that has been used for several applications which includes environmental studies, geotechnical investigations, and explorational projects. This method computes the arrival time of refracted waves when generated from its source. The created waves are detected by a set of geophones fixed on the surveyed ground surface. In this study, seismic refraction approach was employed along the established two profile lines of 40 m length, two profiles for model calibration with coordinates from 5.359296^0 N and 100.303783^0 E to 5.36007^0 N and 100.304376^0 E (Figure 2(a)-2(a')); the others for model verification with coordinates of 5.356350^0 N and 100.302797^0 E to 5.355445^0 N and 100.302666^0 E (Figure 2(b)-2(b')), on the same location as electrical resistivity. The surveying equipment used was ABEM MK8 seismograph, connected to two ports of 12 channels with seismic cables. Each profile line comprised of 24 geophones at 1.0 m geophone spacing with seven (7) shot points. The roll-along protocol adopted, used a 12 kg sledgehammer for seismic signal generation via a metallic plate. The measured seismic refraction dataset was processed using three different software namely, IXRefrac, FIRSTPIX v4.21 and SeisOpt@2D. The DC effect associated with the dataset, was first removed to improve the data quality using IXrefrac, while first arrival signals were picked, and travel time curves plotted with FIRSTPIX. And finally, 2-D seismic pseudo section of velocity spread was generated from SeistOpt@2D and contoured by surfer software as explained by Azwin et al. (2013).

The present study was conducted in two phases. Phase one; involves a correlation between a geophysical parameter of electrical resistivity with laboratory obtained results of soil cohesion and friction angle through simple linear regression equations. In phase two, two geophysical parameters (electrical resistivity and seismic refraction velocity) and the results from the simple linear regression equations are used to develop multiple linear regression modellings which served as the extension of the simple equations. The following subsections contain brief explanations on laboratory and geophysical (non-invasive field) results for simple linear regression equations and multiple linear regression modeling.

BRIEF DETAIL ON THE LABORATORY AND NON-INVASIVE FIELD RESULTS

The geophysical parameter of resistivity (ρ) was obtained based on the 2D imaging technique. The actual values of cohesion (c') and friction angle (ϕ') obtained from geotechnical analysis, were related with true values of the geophysical parameter alongside exact coordinate values (location and elevation). The simple empirical regressions established amongst the ρ with, $c'$and,ϕ' for the soil samples are presented in (1) and (2).

$$c' = 3.157 + 0.015(\rho) \quad (1)$$

$$\varphi' = 53.805 - 0.042(\rho) \quad (2)$$

where ρ (ohm.m), c' (kN/m^2) and ϕ' (degrees). These two equations are used to determine the actual values as it developed from geotechnical laboratory and infield resistivity surveys by Bery (2012). These equations are extended through the incorporation of two geophysical parameters at overlapped points.

OVERLAPPING OF 2D SEISMIC REFRACTION AND 2D ELECTRICAL RESISTIVITY MODELS FOR RAW VALUES GENERATION

In consideration of dissimilar configurations of both seismic and resistivity models, as a consequence of distinct illustration systems of each inversion programs, there is a need for superimposition for equal area coverage by the models (Mota & Monteiro Santos 2010) and data extraction. After the overlap, a dual number of electrical resistivity and seismic velocity values was determined at model grid point. A dataset consisting of values of electrical resistivity (ρ) and seismic refraction velocity (v_p) was subsequently organized in sheets for the multiple linear regression modellings.

MULTIPARAMETER EMPIRICAL RELATIONSHIPS

Consider the least-squares-derived multiple linear regression model having k explanatory parameters (x) and a single response parameter (y) which may be expressed in (3):

$$Y = \beta_0 + \beta_1(x_1) + \beta_2(x_2) + \ldots\ldots + \beta_k(x_k) + \varepsilon \quad (3)$$

whereby β_0 stands for intercept-derived value; β_k is the coefficient of the explanatory parameter x_k, ε stands for the error; and the output parameter is Y. This technique makes the model to converge whenever the squared sum of the deviations among the predicted and measured data is at a lowest limit (Muhammad & Saad 2018). The values of response variables could therefore be calculated for obtained values of predictor variables if the errors happened to have a normal distribution at zero mean with constant variance. The spread of the y is therefore symmetric and bell-like, having a uniform standard deviation at x points (Balarabe et al. 2016).

The study utilized electrical resistivity (ρ) and seismic refraction velocity (v_p) values as the independent variables, while soil cohesion (c') and internal friction angle (ϕ') as the dependent variables. Unluckily, nonlinear behaviour of resistivity and its high variability, and the great variability in values of seismic velocity, constrained the direct usage of the datasets in the multiple regression modeling process. To address this issue, the two different datasets were transformed to logarithmic form (Juhojuntti & Kamm 2015; Meju et al. 2003; Mogaji et al. 2015; Shtivelman 2003). This is to satisfy the regression data diagnostic tests such as linear behaviour, normality of the response parameter, normality and probability of standardized residuals, heteroscedasticity, and outliers, before modeling. The transformed versions of equation (3) involving log-derived resistivity ($Log_{10\,\rho}$) and velocity (Log_{10v}) as independent variables, suitable for the new model parameters, soil cohesion (c') and internal friction angle (ϕ'), to be thus expressed in equations (4) and (5).

$$c' = \beta_0 + \beta_1(Log_{10}\rho) + \beta_2(Log_{10}Vp) \quad (4)$$

$$\phi' = \beta_0 + \beta_1(Log_{10}\rho) + \beta_2(Log_{10}Vp) \quad (5)$$

The outliers in the data sets have been removed using Mahalonobis, Cook's and Centred Leverage distances. Data sets from resistivity (profile 1) and seismic velocity (profile 2) together with values of dependent variables (Equations 1 & 2) were analyzed in SPSS software for multiple linear models' development (Equations 6 & 7) (model calibrations). The constants determined in the models' calibration (Figure 3(a) - 3(a')), have been registered on the different data profiles (Figure 4(a) - (a')) for c' and ϕ' estimations and plotted for interpretation.

Veracity of the developed models has been evaluated via calculation of coefficient of determination (R^2), p-values, and variation inflation factor (VIF), respectively, for model calibration, and error analysis including mean standard error (MSE), root mean square error (RMSE), mean absolute error (MA) and mean absolute percentage error (MAPE) provided in equations (8-11) for model evaluation.

$$c' = -7.502 + 9.555(Log_{10}\rho) - 1.963(Log_{10}Vp) \quad (6)$$

$$\phi' = 83.650 - 26.754(Log_{10}\rho) + 5.497(Log_{10}Vp) \quad (7)$$

$$RMSE = \sqrt{\frac{1}{n}\sum_{i=1}^{n}(y_i - \hat{y}_i)^2} \quad (8)$$

$$MAPE = \frac{100\%}{n}\sum_{i=1}^{n}\left|\frac{y_i - \hat{y}_i}{y_i}\right| \quad (9)$$

$$MSE = \frac{1}{n}\sum_{i=1}^{n}(y_i - \hat{y}_i)^2 \quad (10)$$

$$MAE = \frac{1}{n}\sum_{i=1}^{n}\left|\frac{y_i - \hat{y}_i}{y_i}\right| \quad (11)$$

where y_i is the actual value, $\hat{y}_i$ is the predicted value, and n is the total number of data values.

The efficacy of the developed MLR models in relation to the SLR models in the estimation of soil cohesion and friction angle in 2D form was presented. This was achieved through different error assessments, taken actual values as the estimated soil strength's being products of laboratory analysis, while the predicted values of the soil parameters with the new MLR models.

RESULTS AND DISCUSSION

Interpretations of the 2D tomographic electrical resistivity and seismic refraction data profiles (Figures 3(a)-3(a') & 4(a)-4(a')) pointed to the two subsurface

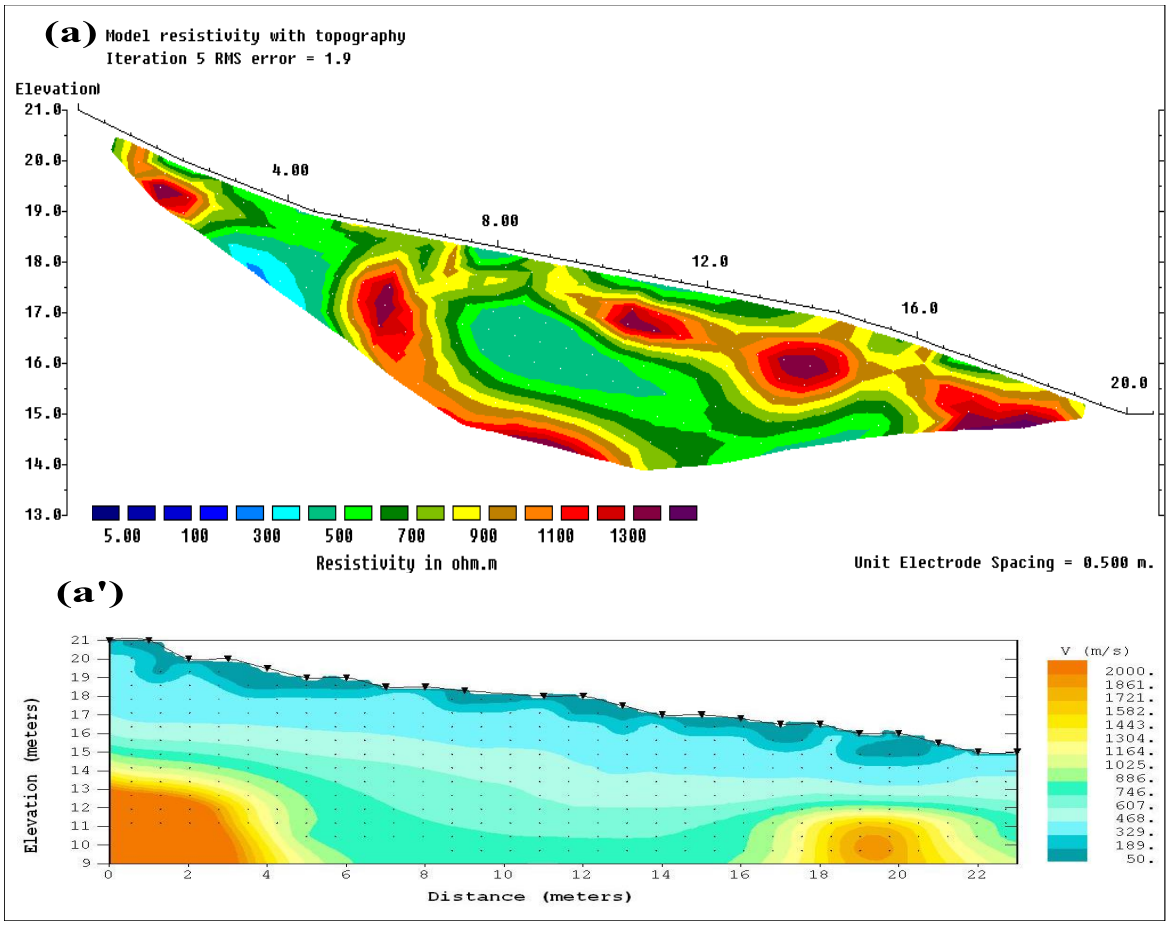

FIGURE 3. 2D inverted geophysical data sets measured along the same straight line for model calibration (a) electrical resistivity profile and (a') seismic refraction profile

resistivity zones (Figures 3(a) & 4(a)), weathered or unsaturated region (>1100 Ωm) and saturated zone (<300 Ω.m) with residual soils (900 Ω.m), depth estimate (1.0 - 4.0 m). While the 2D seismic refraction plots (Figures 3(a') & 4(a')) demonstrated three main subsurface velocity zones, loose soil with boulders (400 - 600 m/s), unsaturated layer (700 - 900 m/s) average depth of 3.0 m, and saturated layer (>1200 m/s) average depth of 6.0 m. The 2D ERT sections showed variant localities due to hydrological conditions and rock compositions which ranged from sands and clays at the upper part, to granitic rocks at lower part of the unsaturated regions and the saturated portion - consolidated sandy silt soil-type. While transition layering of the site has been demonstrated by SRT as zones of low-grade, medium-grade and high-grade materials with compaction levels/velocity values (Al-Heety & Shanshal 2016). The results offer some geophysical insight on the nature of the studied site via the two imaging techniques.

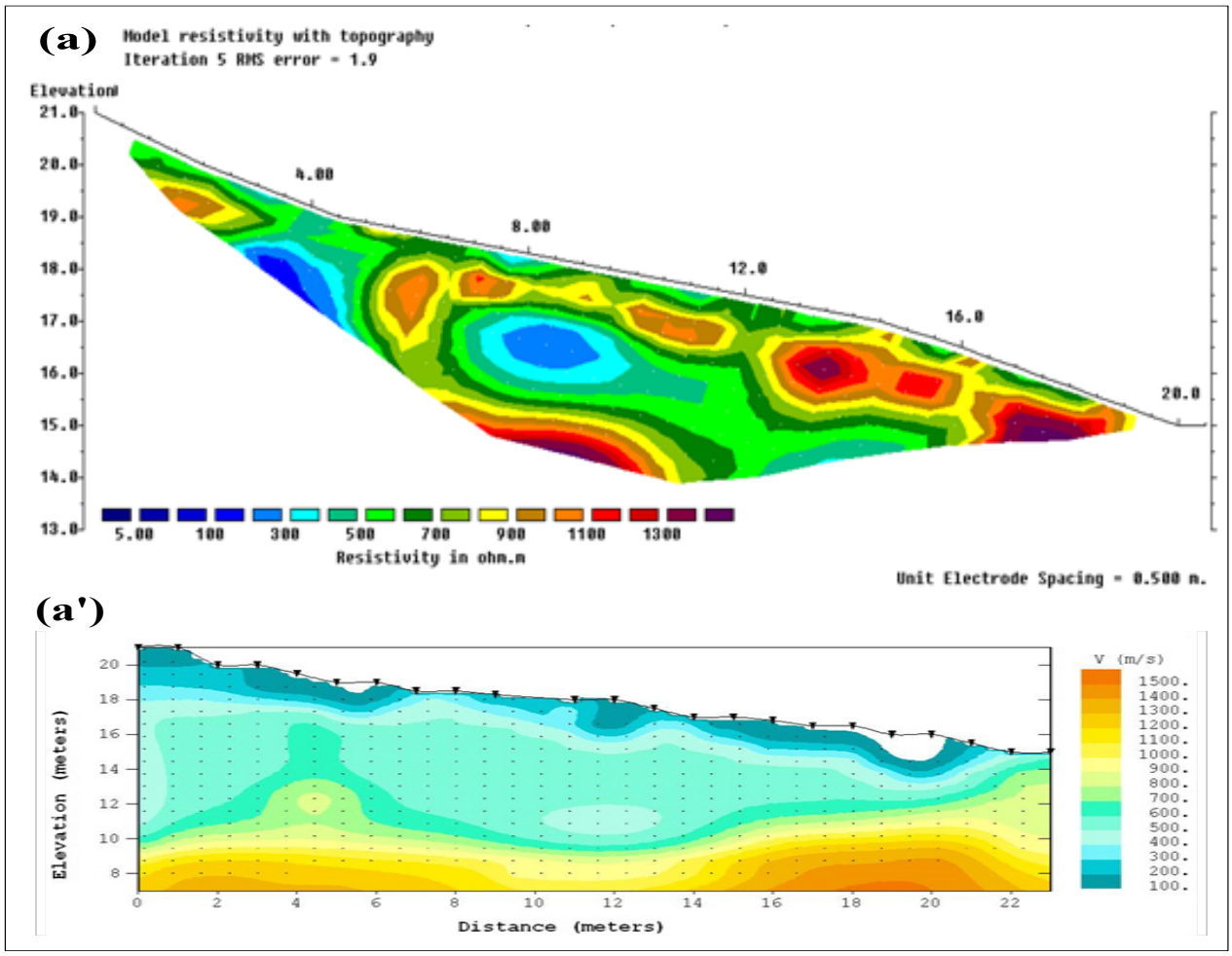

FIGURE 4. 2D inverted geophysical data sets measured along the same straight line for model verification (a) electrical resistivity profile and (a') seismic refraction profile

Figure 5 depicts analysis performed to verify diagnostic regression tests for the datasets. Figure 5(a) demonstrates approximately, linear behaviors, indicating direct proportionalities of assumed values versus measured values, in the normal probability plots of soil cohesion and friction angle data. In a similar manner, approximate uniformity of the residual data spread (Figure 5(b)), suggests a close distribution of the data set, in the span of -2 to +2 on the horizontal axes and from -2 to +1 on the vertical axes across a zero average, for cohesion while those for friction angle ranged from -2 to +2 on all the axis. The tests conducted on the datasets as normal probability plots (Figure 5(a)) and scatter plots (Figure 5(b)), have supported and achieved the approximate linearity and uniform-spread behaviors of the parameters as required by the regression modeling (Hyndman 2018).

Tables 1 and 2 show brief descriptions of the two regression models achieved in this work. The produced coefficients β_0, β_{1} and β_{2}, on substitutions in (6) and (7), resulted into whole models needed for the 2D estimation of soil cohesion and friction angle through geophysical means. The coefficient of determination, R^2 demonstrates the extent of variations in the predicted variables as explained by the predictor variables. The parameters R^2 are obtained to be 0.777 for both soil cohesion and friction angle models. This implies that approximately 78% of change in the subsurface soil cohesion and friction angle was caused by the distributed electrical resistivity and seismic velocity values, consequent of the two models. The unaccounted change (in percentage) coalesced in form of the model residuals, which could be attributed and explained via the difference in data acquisition

pattern, individual inversion procedures, and geological dynamisms. With the high values of R^2 in all the models, designate that the integrated approach was influenced slightly by technical procedures or other geological limitations (hence relying greatly on the measured resistivities and velocities) to predict the cohesion and friction angle. The values of the R^2 found its place in the high reliability side, in accordance with the five stages of absolute strength categorizations of R^2 (Beldjazia & Alatou 2016; Evans 2006), starting from (i) very weak (< 0.04), (ii) weak (0.04-0.15), (iii) moderate (0.16-0.35), (iv) strong (0.36-0.63) and (v) very strong (0.64-1.00). Also, high intercorrelation occurrence between two or more independent variables leads to multicollinearity effect in the datasets. This incident can simply be traced through the variance inflation factor (VIF) value obtained in the analysis. Therefore, the VIF value for the models was 1.185, implying absence of multicollinearity, in contrast with VIF value 10 for highly correlated variables (O'Brien 2007). Another fundamental check was the Durbin-Watson (D-W) test, for detection of autocorrelation in the residual values in the datasets. The Durbin-Watson value for cohesion and friction angle as dependent variables were found as 1.766. Based on a rule of thumb, that a D-W test value must fall between 1.5 and 2.5 to avoid auto correlated effect in the dataset, thus, the value (1.766) signified non autocorrelation in the residuals from regression analysis (Durbin & Watson 1949; Hyndman 2018).

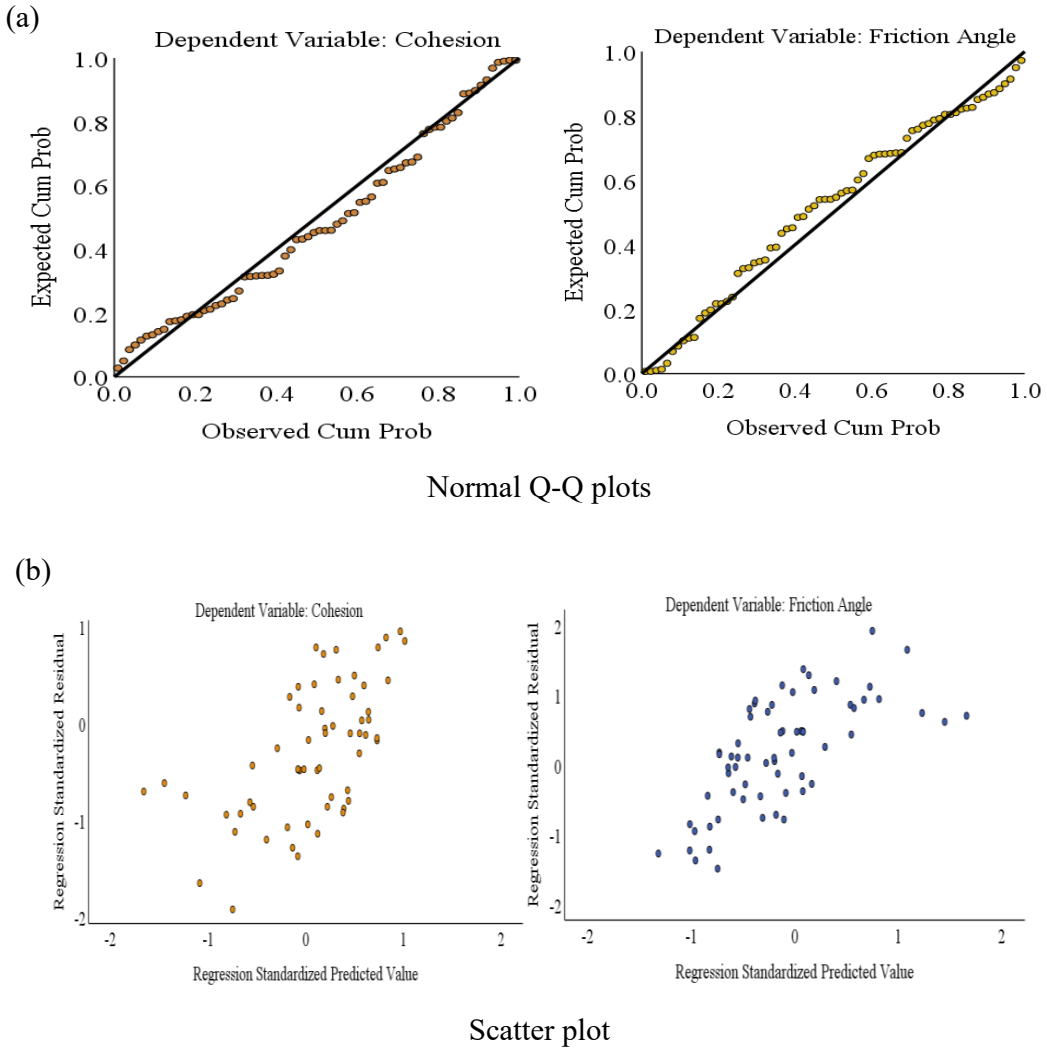

FIGURE 5. Some fundamental regression analysis (a) normal Q-Q plots, and (b) Scatter plots

TABLE 1. The MLR model results for cohesion as dependent variable

Parameters			
Model	Coefficients	*p*-value	VIF
(Constant)	-8.398	0.002	
$Log_{10}(\rho)$	10.598	0.000	1.185
$Log_{10}(Vp)$	-2.635	0.004	1.185

*Dependent variable: Cohesion

*Durbin-Watson value = 1.766; R^2 = 0.777; N =70;

TABLE 2. The MLR model results for friction angle as dependent variable

Parameters			
Model	Coefficients	*p*-value	VIF
(Constant)	86.159	0.000	
$Log_{10}(\rho)$	-29.676	0.000	1.185
$Log_{10}(Vp)$	7.377	0.004	1.185

*Dependent variable: Friction angle

*Durbin-Watson value = 1.7866; R^2 = 0.777; N = 70

Similarly, the F-test proffers an account of whether any of the predictor variables in a model is significant (Tables 1 & 2). The null hypothesis and alternative hypothesis of the test are described such that the coefficients of the models are zeros and at least one of the coefficients is not zero, respectively, for the outcome to be calculated. The *p*-values of the models' parameters determined were found to be in the range of 0 - 0.004 (Tables 1 & 2), explained more of their significance levels in addition to the 95% confidence at which the data were analyzed. With *p*-values 0.05, the null hypothesis has been discarded (Mogaji et al. 2015; Muhammad & Saad 2018), indicating greater contributions of predictor parameters in the outcome estimations and the two models are of considerable importance statistically.

In order to assess and evaluate the accuracies of the developed models for estimation of the outcome variables, error analyses between the actual values (using (1) and (2)) of cohesion and friction angle with the estimated values of cohesion and friction angle (using (6) and (7)), having a total of 43 number of data points, have been conducted. The employed error assessment techniques include MSE, RMSE, MAE and MAPE (Table 3) for models' validations distinctly calculated as 1.4227, 1.1928 kN/m^2, 0.0958 and 9.5846% for soil cohesion and 11.1497, 3.3391 (degree), 0.0882 and 8.8213% for friction angle, respectively. The obtained error values are relatively low which demonstrated that the models are good performing (Muhammad & Saad 2018; Willmott & Matsuura 2006) and can be used on other datasets. Model's reliability is often hinged on the low error margins, as such the values obtained are generally low especially the RMSE values, which indicated a close perfect fit to the data, as a zero value represent a perfect fit, and accounted for outliers' sensitivity (Willmott & Matsuura 2006). The measure of accuracy of models' estimations in percentage was accounted by low values for MAPE (Kim & Kim 2016). Thus, the accuracy forecast was generally good as it further showed narrow margins between the actual and the predicted values for both outcome parameters, as explained by (Abidin & Jaffar 2014).

TABLE 3. Summary of accuracy evaluation the MLR models

Model of MLR	*MSE*	*RMSE*	*MAE*	*MAPE*
Cohesion (kN/m^2)	1.4227	1.1928	0.095846	9.5846
Friction angle (Deg.)	11.1497	3.3391	0.088213	8.8213

Among the two models established and evaluated, soil cohesion has low RMSE value as compared to friction angle, while low value of MAPE was recorded for friction angle against soil cohesion, but values for all the models fall within acceptable limits.

The 2D contour sections of the calculated cohesion and friction angle models were plotted and compared for interpretations (Figures 6 & 7), for model's calibration and validation. The 2D ERT and SRT results were used as a guide in visually classifying the generated 2D soil cohesion and frictional angle sections (Figures 6 & 7) of weathered or unsaturated region (>1100 Ωm) and saturated zone (<300 Ω.m) with residual soils (900 Ω.m), depth estimate of 1.0 - 4.0 m. While the 2D seismic refraction plots (Figures 3(a') & 4(a')) demonstrated three main subsurface velocity zones, loose soil with boulders (400 - 600 m/s), unsaturated layer (700 - 900 m/s) with average depth of 3.0 m, and saturated layer (>1200 m/s) with average depth of 6.0 m. Subsurface geotechnical parameters' distribution were classified into three zones for calibration (Figure 6); low cohesion zone (9 - 12 kN/m^2) relatively located at distance of 3 m, and 3 and 8 m of first and second survey lines, respectively; medium cohesion zone (12 - 15 kN/m) appeared at the centre of the pseudo-sections, 8 m distance and high cohesion (15 - 18 kN/m^2). The low, medium, and high cohesion zones corresponded to saturated, residual soil and unsaturated zones, respectively. Meanwhile, similar behaviour was observed in friction angle values in the areas as; least friction angle having a range of 12 - 21 degrees, medium (21 - 30 degrees), and high (30 - 39 degrees). The low friction angle zone seems scattered at both survey lines around depth of 1 m from surface at distances of 5 m and 10 to 16 m. The results indicated variation in which greater soil cohesion values locations give low friction angle values. Strong cohesion by high values demonstrated great soil particles consistency and geometry/configuration which reduce across the entire soil structure due to the rise in moisture content, thus water variability has great impact on soil strength in the area.

High cohesion zones (Figures 6 & 7) are characterized by soil with large amount of clay material, in this case, very little quantity of sand component in the soil with greater clay component as compared with the medium and low cohesion zones. This property of soil agrees with low amount of moisture content, although the small number of sand grains in the soil profile allows water movement through its pore spaces. It is likely that the little amount of sand grains coupled with interlocking by highly dominant clays in the zones of high cohesive values is in high expectation as compared with literature (Collins & Sitar 2016). The value of soil cohesion varies with water content, grain size, and degree of compaction of soils. Therefore, low cohesion values (Figures 6 & 7) are attributed to relative increase in the amount of moisture content as clay particles tend to separate with more moisture and number of sand grains (Ghosh 2013). The analysis of soils properties from laboratory results showed that 6.01-16.11 kN/m^2 and 10.24-51.47 degree for cohesion and friction angle, respectively, corresponding to the range of resistivity values of 230.677-849.853 (Ohm.m). The details of the analysed soils' properties (cohesion and friction angle) and their corresponding electrical resistivity values are presented in Table 4.

Analysis of the soils' results (Table 4) showed that the soils fall within the saturated zones of relatively moderate resistivity values. The results guided in the interpretation of cohesion with medium values (12.44 - 16.11 kN/m^2) slightly greater compared to that of the models (12-15 kN/m^2), while the low cohesion values (6.01-12.44 kN/m^2) represented a wider range with respect to that of the models (9-12 kN/m^2). The variation could be probably due to the depth of 1.0-1.2 m at which the samples were collected for the laboratory shear test. Also, the soils contain some amount of moisture content making the zone saturated, which facilitated conduction of electric charges within the apertures in the soil network. This leads to the drop of electrical resistivity values. As such, contributed to lessening the strength of the soils with low cohesion values. However, decrease in moisture

quantity results in the uneasy movement of soil particles, leading to high soil compaction and low porosity thus increase soil cohesion (Han et al. 2020; Sadek et al. 2011) and resistivity (Olabode et al. 2020). Similarly, low saturation condition of soils decreased the angle of friction with increase in resistivity values. Increase in saturation condition increases the angle of friction values thereby lessen the strength of soil particles. Therefore, strong soil cohesion leads to strong shear strength of the soil (Yokoi 1968).

TABLE 4. Laboratory analysis results for eleven soil samples with electrical resistivity values

Sample No.	Resistivity ρ(Ohm.m)	Soil's cohesion c' (kN/m²)	Friction angle Ø'(Deg.)
1	275.119	7.35	36.22
2	319.869	8.07	37.28
3	411.589	9.05	40.47
4	230.677	6.01	51.47
5	756.463	14.27	35.08
6	849.853	16.11	10.24
7	585.191	6.87	31.21
8	703.878	10.60	21.40
9	510.298	12.44	25.99
10	724.743	15.27	25.95
11	587.216	15.18	28.00

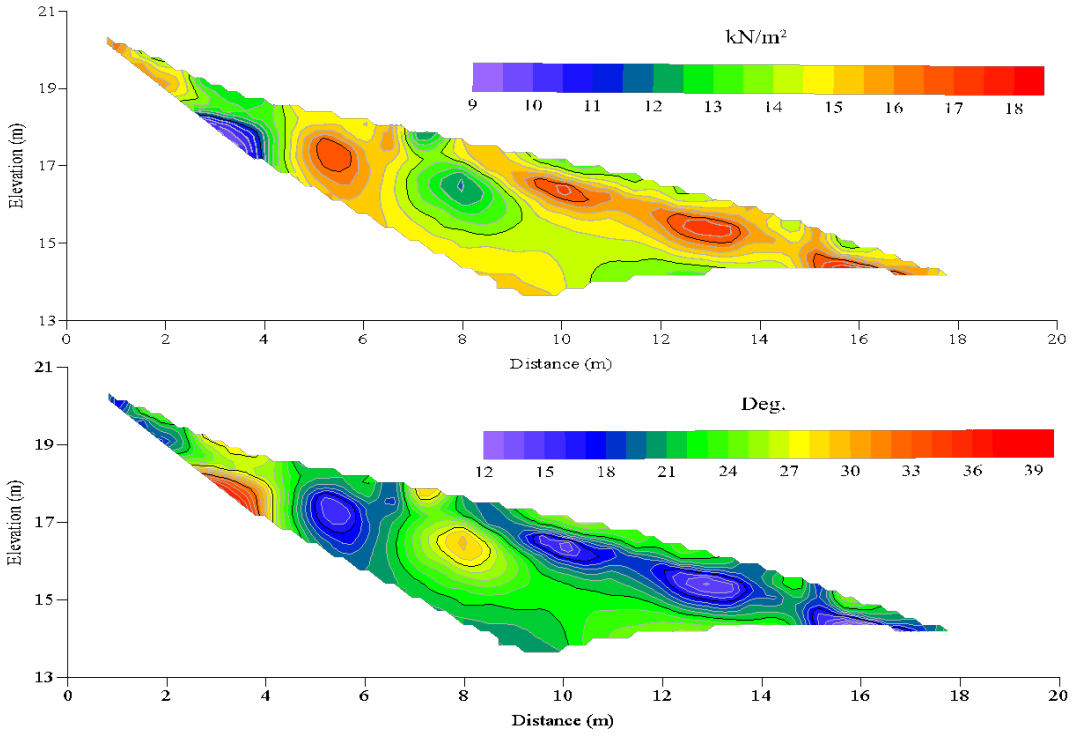

FIGURE 6. Cohesion (Top) and Friction angle (bottom) models for first study line

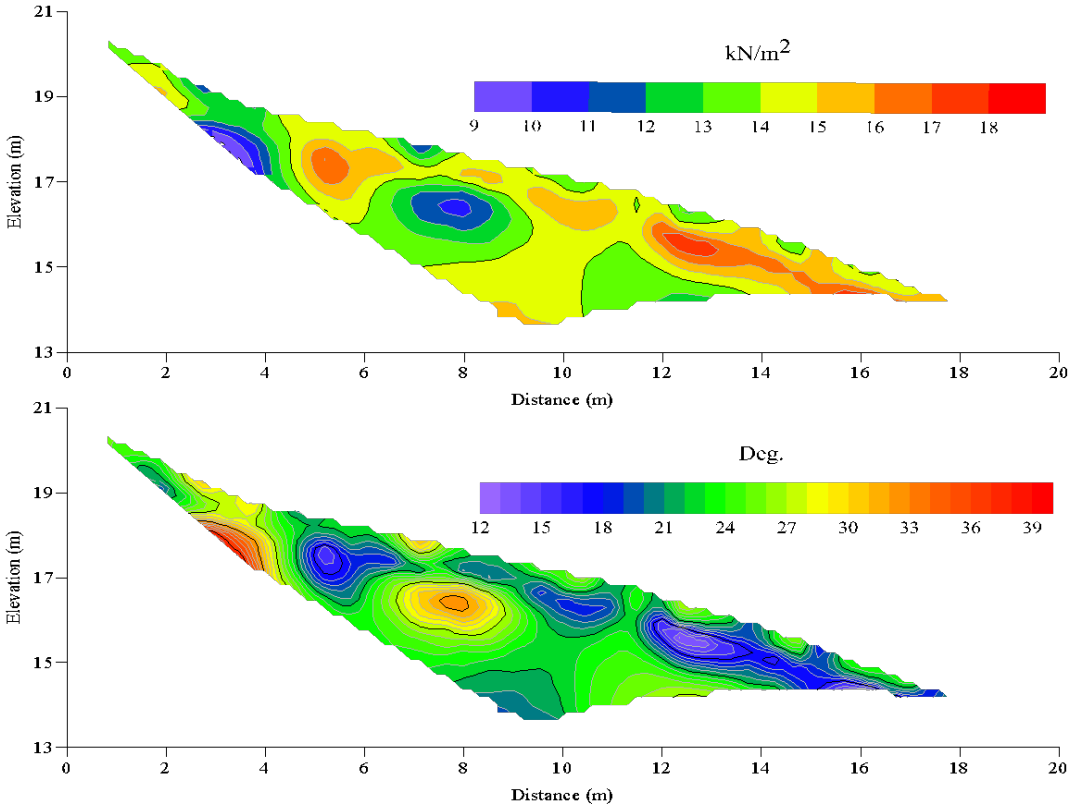

FIGURE 7. Cohesion (Top) and Friction angle (bottom) models for second study line

The soil strength models exhibited the characteristic strength of soils in the investigated area based on integrated results from resistivity and seismic refraction models. It further indicated that low resistivity and high seismic velocity as functions of low cohesion and high friction angle values in clayey sand soil. Hence, the developed soil shear strength models can serve as a reliable predictive tool for near surface investigation with the help of geophysical methods.

CONCLUSION

In this study, the modelling of soil's shear strength was successfully estimated and visualized at the subsurface of the selected study area. These soil's shear strength models are developed using the statistical method called the multiple linear regression. The newly proposed soil's shear strength models were generated from geophysical methods, namely electrical resistivity, and seismic refraction. The MLR model method was used to predict or estimate the distribution of cohesion and friction angle parameters of the soil throughout the survey lines. The developed MLR models were checked for *p*-values and collinearity statistics to identify the evidence in favour of using both geophysical methods. The models demonstrated good performances from the accuracy evaluations conducted between true and predicted soil strength values, using four forecasting methods. Thus, these two models have shown good results and competence in imaging and characterizing the subsurface of studied area in two-dimensional form. Hence, covered more regions compared to traditional drilling and other destructive approaches. Also, the models being non-invasive, quick, and cost-effective, can be employed at initial stage for site and engineering projects.

ACKNOWLEDGEMENTS

The authors are thankful to Universiti Sains Malaysia for providing the equipment and technical staff of Geophysics that assisted in data acquisition. The first author extends his appreciation to TETFUND for the financial aid for the study. The authors are appreciative to the anonymous reviewers for constructive inputs towards improving the manuscript.

REFERENCES

Abdul Hamid, F.A.Z., Abu Bakar, A.F., Ng, T.F., Ghani, A.A. & Mohamad Zulkefly, M.T. 2019. Distribution and contamination assessment of potentially harmful elements (As, Pb, Ni, Cd) in top soil of Penang Island, Malaysia. *Environmental Earth Sciences* 78(21): 1-12.

Abidin, S.N.Z. & Jaffar, M.M. 2014. Forecasting share prices of small size companies in Bursa Malaysia using geometric brownian motion. *Applied Mathematics & Information Sciences* 8(1): 16632699.

Adewoyin, O., Joshua, E., Akinyemi, M.L., Maxwell, O. & Aanuoluwa, A. 2021. Evaluation of geotechnical parameters of reclaimed land from near-surface seismic refraction method. *Heliyon* 7(4): e06765.

Ahmad, F., Yahaya, A.S. & Farooqi, M.A. 2006. Characterization and geotechnical properties of Penang residual soils with emphasis on landslide. *American Journal of Environmental Sciences* 2(4): 121-128.

Al-Heety, A.H. & Shanshal, Z.M. 2016. Integration of seismic refraction tomography and electrical resistivity tomography in engineering geophysics for soil characterization. *Arabian Journal of Geosciences* 9(1): 1-11.

Alimoradi, A., Moradzadeh, A., Naderi, R. & Salehi, M.Z. 2008. Prediction of geological hazardous zones in front of a tunnel face using TSP-203 and artificial neural networks. *Tunnelling and Underground Space Technology* 23(6): 711-717.

Azwin, I., Saad, R. & Nordiana, M. 2013. Applying the seismic refraction tomography for site characterization. *Procedia* 5: 227-231.

Balarabe, M., Abdullah, K., Nawawi, M. & Khalil, A.E. 2016. Monthly temporal-spatial variability and estimation of absorbing aerosol index using ground-based meteorological data in Nigeria. *Atmospheric and Climate Science* 6(3): 425-444.

Beldjazia, A. & Alatou, D. 2016. Precipitation variability on the Massif Forest of Mahouna (North Eastern-Algeria) from 1986 to 2010. *International Journal of Management Science and Business Research* 5(3): 21-28.

Brixova, B., Mosna, A. & Putiska, R. 2018. Applications of shallow seismic refraction measurements in the Western Carpathians (Slovakia): Case studies. *Contributions to Geophysics and Geodesy* 48(1): 1-21.

Caterina, D., Beaujean, J., Robert, T. & Nguyen, F. 2013. A comparison study of different image appraisal tools for electrical resistivity tomography. *Near Surface Geophysics* 11(6): 639-657.

Collins, B.D. & Sitar, N. 2016. Geotechnical properties of cemented sands in steep slopes. *Journal of Geotechnical and Geoenvironmental Engineering* 135(10): 1359-1366.

Durbin, J. & Watson, G.S. 1949. Testing for serial correlation in least squares regression: I. *Biometrika* 37(3/4): 409-428.

Gabr, A., Murad, A.A., Baker, H., Bloushi, K.M.A., Arman, H. & Mahmoud, S. 2012. The use of seismic refraction and electrical techniques to investigate groundwater aquifer, Wadi Al-Ain, United Arab Emirates (UAE). In *International Conference Water Resources and Wetland.* Tulcea, Romania.

Ghosh, R. 2013. Effect of soil moisture in the analysis of undrained shear strength of compacted clayey soil. *Journal of Civil Engineering and Construction Technology* 4(1): 23-31.

Guo, N. & Zhao, J. 2013. The signature of shear-induced anisotropy in granular media. *Computers and Geotechnics* 47: 1-15.

Han, Z., Li, J., Gao, P., Huang, B., Ni, J. & Wei, C. 2020. Determining the shear strength and permeability of soils for engineering of new paddy field construction in a hilly mountainous region of Southwestern China. *International Journal of Environmental Research and Public Health* 17(5): 1555.

Horn, R. 2003. Stress - strain effects in structured unsaturated soils on coupled mechanical and hydraulic processes. *Geoderma* 116: 77-88.

Ismail, M.A.M., Majid, T.A., Goh, C.O., Lim, S.P. & Tan, C.G. 2019. Geological assessment for tunnel excavation under river with shallow overburden using surface site investigation data and electrical resistivity tomography. *Measurement* 144: 260-274.

Juhojuntti, N. & Kamm, J. 2015. Joint inversion of seismic refraction and resistivity data using layered models - Applications to groundwater investigation. *Geophysics* 80(1): EN43-EN55.

Junior, S.B.L., Prado, R.L. & Mendes, R.M. 2012. Application of multichannel analysis of surface waves method (MASW) data acquisition. *Revista Brasileira de Geoisica* 30(2): 213-224.

Kim, S. & Kim, H. 2016. A new metric of absolute percentage error for intermittent demand forecasts. *International Journal of Forecasting* 32(3): 669-679.

Martínez, K. & Mendoza, J.A. 2011. Urban seismic site investigations for a new metro in central Copenhagen: Near surface imaging using reflection, refraction and VSP methods. *Physics and Chemistry of Earth, Parts A/B/C* 36: 1228-1236.

Mcclymont, A., Bauman, P., Johnson, E. & Pankratow, L. 2016. Geophysical applications to construction engineering projects. *Recorder* 41(4): 16-22.

Meju, M.A., Gallardo, L.A. & Mohamed, L.K. 2003. Evidence for correlation of electrical resistivity and seismic velocity in heterogeneous near-surface materials. *Geophysical Research Letters* 30(7): 7-10.

Mitchell, J.K. & Soga, K. 2005. *Fundamentals of Soil Behavior.* 3rd ed. New Jersey: John Wiley & Sons Inc.

Mogaji, K.A., Lim, H.S. & Abdullah, K. 2015. Modeling of groundwater recharge using a multiple linear regression (MLR) recharge model developed from geophysical parameters: A case of groundwater resources management. *Environmental Earth Sciences* 73(3): 1217-1230.

Mota, R. & Monteiro Santos, F.A. 2010. 2D sections of porosity and water saturation from integrated resistivity and seismic surveys. *Near Surface Geophysics* 8(6): 575-584.

Muhammad, S.B. & Saad, R. 2018. Linear regression models for

estimating true subsurface resistivity from apparent resistivity data. *Journal of Earth System Science* 127(5): 64.

Nguyen, F., Garambois, S., Jongmans, D., Pirard, E. & Loke, M.H. 2005. Image processing of 2D resistivity data for imaging faults. *Journal of Applied Geophysics* 57: 260-277.

O'Brien, R.M. 2007. A caution regarding rules of thumb for variance inflation factors. *Quality & Quantity* 41: 673-690.

Okpoli, C.C. 2013. Sensitivity and resolution capacity of electrode configurations. *International Journal of Geophysics* 2013: 608037.

Olabode, O.P., San, L.H. & Ramli, M.H. 2020. Analysis of geotechnical-assisted 2-D electrical resistivity tomography monitoring of slope instability in residual soil of weathered granitic basement. *Frontier in Earth Science* 7: 1-15.

Owusu-nimo, F. & Boadu, F.K. 2020. Evaluating effective stress conditions in soils using non-invasive electrical measurements - laboratory studies. *Journal of Applied Geophysics* 174: 103961.

Sadek, M.A., Chen, Y. & Liu, J. 2011. Simulating shear behavior of a sandy soil under different soil conditions. *Journal of Terramechanics* 48(6): 451-458.

Shahangian, S. 2011. Variable cohesion model for soil shear strength evaluation. In *14th Pan-American Conference on Soil Mechanics and Geotechnical Engineering*. Toronto, Canada.

Shahrukh, M., Soupios, P., Papadopoulos, N. & Sarris, A. 2012. Geophysical investigations at the istron archaeological site, Eastern Crete, Greece using seismic refraction and electrical resistivity tomography. *Journal of Geophysics and Engineering* 9(6): 749-760.

Shtivelman, V. 2003. Application of shallow seismic methods to engineering, environmental and groundwater investigations. *Bollettino di Geofisica Teorica ed Applicata* 44(3-4): 209-222.

Van Hoorde, M., Hermans, T., Dumont, G. & Nguyen, F. 2017. 3D electrical resistivity tomography of karstified formations using cross-line measurements. *Engineering Geology* 220(13): 123-132.

Wei, Y., Wu, X., Xia, J., Miller, G.A., Cai, C. & Guo, Z. 2019. The effect of water content on the shear strength characteristics of granitic soils in South China. *Soil & Tillage Research* 187: 50-59.

Whiteley, J.S., Chambers, J.E., Uhlemann, S., Boyd, J., Cimpoiasu, M.O., Holmes, J.L., Inauen, C.M., Watlet, A., Hawley-Sibbett, L.R., Sujitapan, C., Swift, R.T. & Kendall, J.M. 2020. Landslide monitoring using seismic refraction tomography - the importance of incorporating topographic variations. *Engineering Geology* 268: 105525.

Willmott, C.J. & Matsuura, K. 2006. On the use of dimensioned measures of error to evaluate the performance of spatial interpolators. *International Journal of Geographical Information Science* 20(1): 89-102.

Wu, Z., Niu, Q., Li, W., Lin, N.H. & Liu, S. 2018. Ground stability evaluation of a coal-mining area: A case study of Yingshouyingzi mining area, China. *Journal of Geophysics and Engineering* 15(5): 2252-2265.

Yeh, H.F., Lin, H.I., Wu, C.S., Hsu, K.C., Lee, J.W. & Lee, C.H. 2015. Electrical resistivity tomography applied to groundwater aquifer at downstream of Chih-Ben Creek Basin, Taiwan. *Environmental Earth Science Earth Science* 73(8): 4681-4687.

Yokoi, H. 1968. Relationship between soil cohesion and shear strength. *Soil Science and Plant Nutrition* 14(3): 89-93.

Bala Balarabe, Andy Anderson Bery* & Teoh Ying Jia
School of Physics
Universiti Sains Malaysia
11800 Penang
Malaysia

Bala Balarabe
Department of Physics
Faculty of Physical Sciences
Ahmadu Bello University, Zaria
Nigeria

Amin Esmail Khalil
Geology Department, Faculty of Science
Helwan University
Ain Helwan, Cairo
Egypt

*Corresponding author; email: andersonbery@yahoo.com.my

Received: 18 January 2021
Accepted: 18 June 2021